# Coseismic versus interseismic ground deformations, fault rupture inversion and segmentation revealed by 2003 *Mw* 6.8 Chengkung earthquake in eastern Taiwan

Y. M. Wu,[1] Y. G. Chen,[1] T. C. Shin,[2] H. Kuochen[2] C. S. Hou,[3] J. C. Hu,[1] C. H. Chang,[2] C. F. Wu,[2] and T. L. Teng[4]

Received 23 September 2005; revised 30 November 2005; accepted 6 December 2005; published 25 January 2006.

[1] The 2003 Chengkung earthquake (*Mw* 6.8) provided diagnostic evidence for a source model showing the deformation process of the seismogenic Chihshang fault in eastern Taiwan. The aftershocks show a fault-bend at a depth of 18 km. Coseismic ground displacements recorded by strong-motion records allow us to deduce instant rupturing of this event. Our resulting model shows a fault length of ~33 km and dip-slip dominant rupture on fault-plane deeper than 18 km. Estimated coseismic displacements constrain two fault planes: one at 5–18 km depth dipping 60°E and 18–36 km depth dipping 45°E. The uppermost fault-plane of the Chihshang Fault (0–5 km) did not break immediately after the main shock; however, it may have a major role in after-slip and even interseismic ground deformation. The Taiyuan basin developed in the hanging wall is a geomorphic feature consistent with and adequately explained by coseismic ground displacements.
**Citation:** Wu, Y. M., Y. G. Chen, T. C. Shin, H. Kuochen, C. S. Hou, J. C. Hu, C. H. Chang, C. F. Wu, and T. L. Teng (2006), Coseismic versus interseismic ground deformations, fault rupture inversion and segmentation revealed by 2003 *Mw* 6.8 Chengkung earthquake in eastern Taiwan, *Geophys. Res. Lett.*, *33*, L02312, doi:10.1029/2005GL024711.

## 1. Introduction

[2] Large earthquakes commonly occur in eastern Taiwan due to the vigorous arc-continent collision with a converging rate of 7 to 8 cm/year [*Suppe*, 1981; *Ho*, 1986; *Tsai*, 1986; *Angelier et al.*, 1997, 2000] (Figure 1). The fault system in the Longitudinal Valley (LV) is one of the sutures in the collision zone and it is characterized by high seismicity [*Tsai*, 1986; *Shyu et al.*, 2005]. Two dominant thrust faults, i.e., the Central Range fault (CNF) and Coastal Range fault (COF), bound the mountain fronts of the Central Range and Coastal Range (CR) (Figure 1) [*Biq*, 1965; *Angelier et al.*, 1997, 2000; *Lee et al.*, 2001, 2003]. Using the data of the earthquake sequence of the 2003 Chengkung earthquake (*Mw* 6.8, On Dec. 10), this paper analyzes the southern segment of the COF, namely the Chihshang fault (CSF; Figure 1). Both geological and geophysical data indicate that the CSF is an oblique-slip reverse fault, striking roughly perpendicular to the plate convergence direction [*Angelier et al.*, 1997, 2000; *Lee et al.*, 2001, 2003; *Kuochen et al.*, 2004].

[3] On December 10, 2003, the Chengkung earthquake occurred at a focal depth in the range of 10–25 km as reported by the CWB (Central Weather Bureau of Taiwan), BATS-CMT (Broadband Array in Taiwan for Seismology), Harvard-CMT, and later study [*Kuochen et al.*, 2006]. Its strong motion resulted in landslides, rock falls, and construction damages in the epicentral area. The focal mechanism determined from first-motion shows a nearly pure thrust event (037°, 50°, 94°) [*Kuochen et al.*, 2006]. Scientists were surprised by the inconsistency between the first-motion result (short-period recordings) and the oblique slip (teleseismic long-period recordings) reported by Havard-CMT (Rake = 69°). It appears that the strike-slip displacement occurred immediately after the initial first-motion of the nucleating thrusting. These observations lead to two questions: What was the actual rupturing process of this event? And how did the dip-slip motion transfer into a strike-slip motion? One way to address these questions is to simulate the rupture of the main shock by coseismic records on the ground surface. Fortunately, significant crustal deformations were recorded by nearby strong-motion stations and a GPS network, although no visual surface rupture was reported. We have intentionally avoided the GPS data because of the fewer continuous GPS stations and contaminated results of campaign GPS by after-slip. To have enough spatial distribution to constrain the coseismic surface displacement, we chose the strong-motion records from the Taiwan Strong-Motion Instrumentation Program (TSMIP) of the CWB as our primary data set. The resultant horizontal vectors are generally consistent with the coseismic GPS observations, but entirely different from the interseismic velocities (Figures 1 and 4a) [*Yu et al.*, 1997; *Yu and Kuo*, 2001], which show systematic northwestward vectors for all of the stations within CR (Figure 1). In contrast, the 2003 coseismic displacements display a radial pattern with a center located within the southern CR. Hence additional questions arise: What are the mechanisms and relationships between the interseismic and coseismic crustal deformations? Are those deformations given by the same fault?

## 2. Structural Framework and Neotectonics

[4] The arc-continent collision in Taiwan began in the late Miocene (inset of Figure 1) [*Ho*, 1986; *Teng*, 1990]. The CR in eastern Taiwan is in fact a remnant of the

[1]Department of Geosciences, National Taiwan University, Taipei, Taiwan.
[2]Central Weather Bureau, Taipei, Taiwan.
[3]Central Geological Survey, Taipei, Taiwan.
[4]Department of Earth Sciences, University of Southern California, Los Angeles, California, USA.


0094-8276/06/2005GL024711$05.00

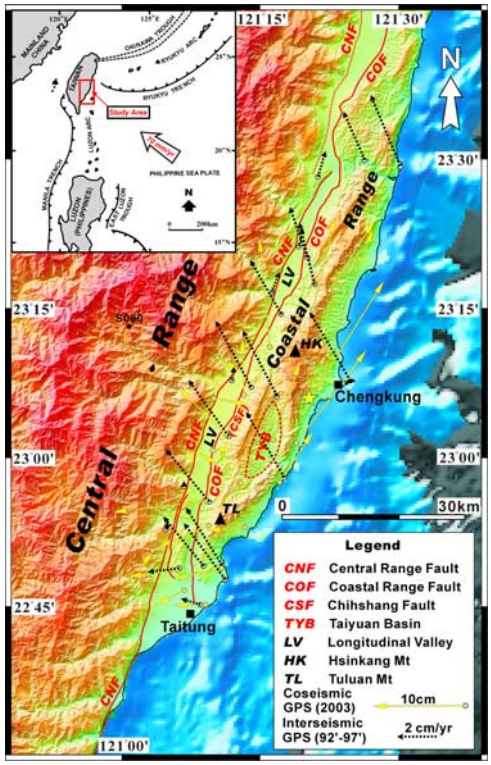


**Figure 1.** Shaded relief DEM map of eastern Taiwan. The vectors show the interseismic velocities relative to S080 (black dash) and coseismic displacements (yellow). The southern CR is characterized by the topographic highs of HK and TL and the TYB basin. Inset shows the tectonic settings of Taiwan.

accreted Luzon arc (Figure 1). The interseismic GPS-based velocities show a general convergent direction of 303° to 324° [*Yu and Kuo*, 2001], not exactly perpendicular to the orientation of the geological features. This relationship implies that the developed major faults should be thrusts with strike-slip components. As shown by previous GPS study, shortening along the COF is ~2 cm/yr across the fault with different slip directions [*Yu and Kuo*, 2001]; however, the hanging wall undergoes negligible shortening. The southern segment of the COF (CSF) has no clearly defined termination to its south or north. Field measurements indicate that it is an oblique-reverse fault [*Angelier et al.*, 1997]. During the largest recent earthquake (Ms 7.1) in 1951, only a few ambiguous surface ruptures were reported; thus many scientists believed that no rupture was associated with this event [*Hsu*, 1962; *Chung*, 2003]. Based on this and its rapid aseismic creeping rate [*Angelier et al.*, 1997, 2000; *Lee et al.*, 2001, 2003; *Yu et al.*, 1990; *Yu and Liu*, 1989], geologists therefore predicted less coseismic slip for the CSF. The fault-plane geometry has been studied using the distribution of background seismicity during 1998–2001 [*Lee et al.*, 2003; *Kuochen et al.*, 2004], imaging a listric subsurface extension down to a depth of 30 km with dips of 60° in depths <18 km and to 45° at greater depth. In 2003, the extensive database of TSMIP, therefore, provides a unique opportunity to better define the coverage of this fault. The computed hypocenter of the Chengkung main shock and the 372 relocated aftershocks ($M_L$ > 3.0; until Dec. 31, 2003; Figure 2) also show similar east-dipping listric distributions.

## 3. 2003 Coseismic Displacements

[5] The TSMIP stations are operated under low-gain mode with ~650 modern digital accelerographs installed at free-field sites and the signals are sampled at 200 Hz. The non-linear baseline of the acceleration and the trend in the velocity indicate that ground tilt occurred during the earthquake [*Boore*, 2001; *Chung and Shin*, 1999]. The displacement of the station itself was obtained by mean of subtracting the acceleration trace according to the pre-event record (Figure 3a) (Y. M. Wu and C. F. Wu, Recovery coseismic deformation from strong-motion records, submitted to *Terrestrial, Atmospheric and Ocean Sciences*, 2005) and then integrating once for velocity (Figures 3b and 3c) and twice for displacement (Figures 3d and 3e). In total 38 stations are processed, covering the coseismic ground displacement field of the 2003 event. For example, the corrected seismograms of the north-south component of TTN034 give a coseismic northward displacement of 7.6 cm (Figure 3e). The general standard error in this study is ~0.26 cm. The resultant horizontal components (Figure 4a) demonstrate that the northern area generally moved northeastward, with values from 3–4 cm in the LV up to 7–10 cm

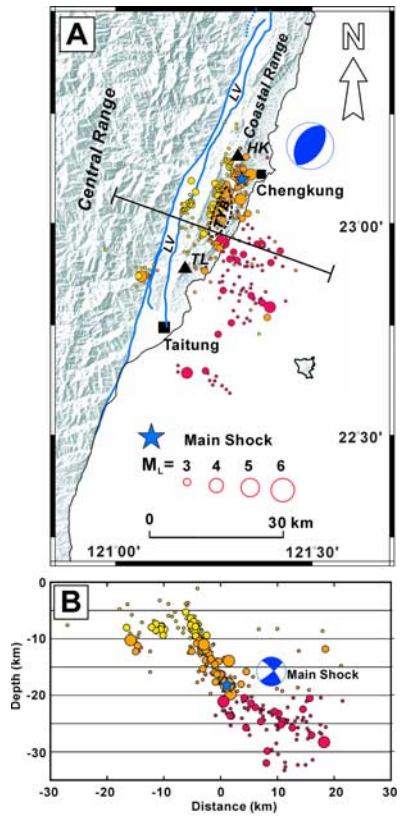


**Figure 2.** (a) Map showing the epicenters of the 2003 Chengkung earthquake sequence distributed primarily between and to the east of mountains HK and TL. (b) The CSF is a listric shape fault, coincident with the previously reported results.

in the eastern coast. However, in the southern area, the vectors turn southwestward, with values decreasing to 2–3 cm. Near the CSF, east-west shortening is dominant but the values become less than 1 cm. In contrast, vertical displacements (Figure 4b) show that the northern areas were lifted up to ~20 cm, whereas the southern area almost stood still except for a few areas lifted up to 2 cm (Figure 4b). Note that the larger displacements were concentrated near the epicenter, implying that the crustal movements are closely related to the rupture of the main shock. On the whole, the pattern of horizontal displacements is similar to the GPS results except for the near-fault region that shows less shortening in the seismic data (Figures 1 and 4a), indicating the great reliability of our data. The significantly larger shortening in the near fault stations probably reflects considerable after-slip included in the GPS results due to the longer time span between GPS occupations. We deliberately chose strong-motion records to avoid the after-slip interference. Also, an additional advantage of our method is that the seismic data provide more accurate vertical displacements than the GPS data since the sub-centimeter accuracy is obtained.

## 4. Dislocation Fault Model

[6] The 120 above-derived ground displacements are used to invert the rupture dislocation model of the main shock. The method is modified mainly after that of the previous study [*Okada*, 1992]. Under assumption of uniform dislocation, we did trial-and-error for the position and area for single fault-plane. Obviously a simple flat fault-plane cannot produce the ground-deformation pattern (Figure 4). We therefore assume a fault-plane strikes 020°, parallel to the LV, with a bend at a depth of 18 km which is

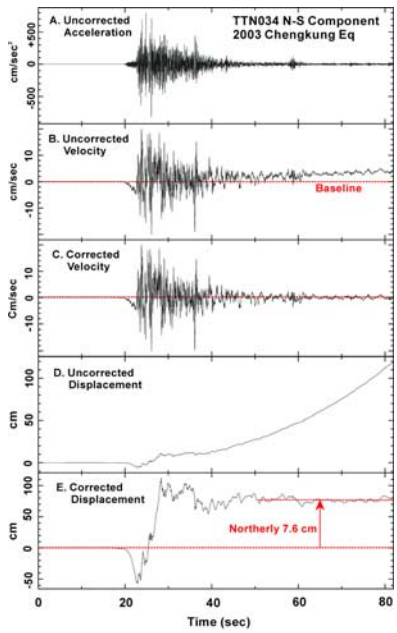


**Figure 3.** The procedures for the conversion of a strong-motion record into site displacement. (a) The original accelerograph record can be integrated into (b) and (c) velocity and (d) and (e) displacement after their baseline corrections.

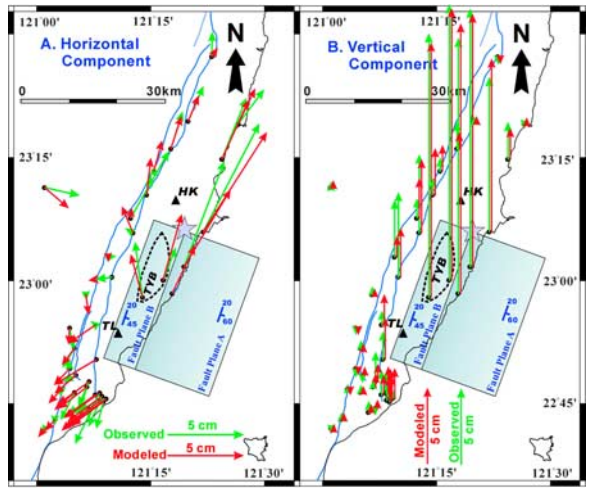


**Figure 4.** Maps showing the coseismic displacements from the strong-motion records for both (a) the horizontal and (b) the vertical components. The yellow squares are the projections of the modeled fault-planes (see details in text). The arrows show the displacements, including the modeled (red) and observed (green).

defined by the aftershock distribution and the geological map [*Central Geological Survey*, 2000a, 2000b]. The fault-plane dips 60° and 45° above and below the bend respectively. The lower and upper fault-planes are abbreviated as Fault A and B, respectively, in Figure 4 and Table 1. For the best fit with the coseismic ground deformation both fault-planes extend 33 km at most. The fault A and B ruptured only within depths of 18–36 km and 5–18 km, respectively. Other relevant parameters are given in Table 1. Our results show that the major slip of 61.6 cm occurred on the Fault A with a rake of 81.7°, which is consistent with the first-motion estimate. The Fault B slipped 26 cm with a rake of 47.3°. Based on the area and the slip of the ruptured surface of each fault, we estimate *Mw* 6.7 and *Mw* 6.3 for Fault A and B, respectively. The total *Mw* is about 6.8, agreeing with the result of the moment tensor inversion solution from the Harvard CMT database and indicating that the seismic energy was mainly released by Fault A. Furthermore, by the best-fit model we conducted a forward computation for the ground displacements, which is consistent with the observed values for both the horizontal and the vertical components (Figures 1, 4a, and 4b; auxiliary material[1]).

[7] Our results confirm again that the southern COF (CSF) bends at a depth of 18 km, from 60° to 45° (Figure 2). Also, the earthquake rupture initialized as a dip slip event as estimated by the focal mechanism of the first-motion (Table 1). This further suggests that the CSF is horizontally segmented. In addition, it is worth noting that the uppermost part (0–5 km) of the CSF did not participate in the co-seismic slip in 2003 event. However, it did give a significant amount of after-slip according to the GPS measurements (Figure 1) [*Chen et al.*, 2005]. In terms of the interseismic velocity field (Figure 1) [*Yu and Kuo*, 2001], the uniform westerly pointing vectors only show significant creeping along the CSF but carry no information about the

[1]Auxiliary material is available at ftp://ftp.agu.org/apend/gl/2005GL024711.

**Table 1.** Parameters of Fault Model

| | Left Bottom Point | | | | | | | | |
|---|---|---|---|---|---|---|---|---|---|
| | Long., E | Lat., N | Depth, km | Strike | Dip | Length, km | Width, km | Strike Slip,[a] cm | Dip Slip,[b] cm |
| A | 121.216° | 22.820° | 18.0 | 020° | 45° | 33.0 | 25.0 | 8.9 | 61.0 |
| B | 121.147° | 22.843° | 5.0 | 020° | 60° | 33.0 | 15.0 | 17.6 | 19.1 |

[a]Hanging wall, positive for 020° direction.
[b]Hanging wall, positive for up-throwing.

existence of the Fault A and B. Both the after-slip and the interseismic slip (Figure 1) show large east-west shortening along the CSF, which is different from the coseismic slips given by Fault A and B model. We tentatively attribute these to the shallower counterpart (0–5 km) of the seismogenic fault-planes (5–18 and 18–36 km) in response to cumulated stress transferred from the deeper part after an earthquake event. In this case, the uniform direction pattern of the interseismic vectors implies that this shallow fault should not be horizontally segmented. This hypothesis, however, needs additional verification by the re-evaluation of more interseismic GPS data, as well as by the modeling of its slip field. As a whole, the CSF can be vertically divided into at least three fault-planes: 0–5, 5–18, and 18–36 km. The deepest one, Fault A, is undoubtedly the principal seismogenic source.

## 5. Other Observations and Conclusion

[8] To further consider the present geomorphic features and geologic configuration related to the CSF, we found that the crest lines of the CR show a parallel, tight pattern in the north that is governed by the west vergent and imbricated thrust sheets (Figure 1). Based on the geological map, the mountain ranges are nearly all composed of volcanic bodies, while the lowlands are sandy/muddy sedimentary sequences that were previously deposited in the fore- or intra-arc [*Chen and Wang*, 1986]. In the study area (between the Hsinkang and Tuluan Mountains of the CR) (Figures 1, 4a, and 4b) the mountains split into two crests forming an olive-shaped basin (TYB in Figures 1 and 4). This shape should not be the original one since the mountains were severely stretched during the collision. The present basin shape must reflect the finite strain of the recent tectonic deformation. The interseismic GPS velocities (Figure 1) [*Yu and Kuo*, 2001] can explain neither the creation nor the olive-shape of the basin. On the contrary, the coseismic slips provided by the 2003 event can apparently solve this discrepancy. The profile across the TYB (Figure 4) clearly shows a pop-up motion in response to the listric shape of the CSF and to keep the basin configuration. The elongate shape of the TYB can be further explained by a simple shear caused by differential displacements across the CR. Only if the TYB remains, must the coseismic contribution be equal to or greater than that of the interseismic shortening; otherwise, this basin could not have formed and be preserved.

## References


Angelier, J., H. T. Chu, and J. C. Lee (1997), Shear concentration in a collision zone: Kinematics of the active Chihshang Fault, Longitudinal Valley, eastern Taiwan, *Tectonophysics*, *274*, 117–144.

Angelier, J., H. T. Chu, J. C. Lee, and J. C. Hu (2000), Active faulting and earthquake risk: The Chihshang Fault case, Taiwan, *J. Geodyn.*, *29*, 151–185.

Biq, C. (1965), The east Taiwan rift, *Petrol. Geol. Taiwan*, *4*, 93–106.

Boore, D. M. (2001), Effect of baseline corrections on displacements and response spectra for several recordings of the 1999 Chi-Chi, Taiwan, earthquake, *Bull. Seismol. Soc. Am.*, *91*, 1199–1211.

Central Geological Survey (2000a), Geological map of Taiwan, scale 1:500000, Taiwan.

Central Geological Survey (2000b), Active fault map of Taiwan, scale 1:500000, Taiwan.

Chen, W. S., and Y. Wang (1986), *Coastal Range Geology in Eastern Taiwan* (in Chinese with English abstract), Cent. Geol. Surv., Taipei, Taiwan.

Chen, H. Y., S. B. Yu, L. C. Kuo, and C. C. Liu (2005), Coseismic and postseismic displacement of the 10 December 2003 (*Mw* 6. 8) Chengkung earthquake, eastern Taiwan, *Earth Planet Space*, *57*, 1–17.

Chung, J. K., and T. C. Shin (1999), Implications of the rupture process from the displacement distribution of strong motions recorded during the 21 September 1999 Chi-Chi, Taiwan earthquake, *Terr. Atmos. Oceanic Sci.*, *10*, 777–786.

Chung, L. H. (2003), Surface rupture reevaluation of the 1951 earthquake sequence in the central Longitudinal Valley and neotectonic implications (in Chinese with English abstract), M.S. diss., 138 pp., Inst. of Geosci., Natl. Taiwan Univ., Taiwan.

Ho, C. S. (1986), A synthesis of the geologic evolution of Taiwan, *Tectonophysics*, *125*, 1–16.

Hsu, T. L. (1962), Recent faulting in the Longitudinal Valley of eastern Taiwan, *Mem. Geol. Soc. China*, *1*, 95–102.

Kuochen, H., Y. M. Wu, C. H. Chang, J. C. Hu, and W. S. Chen (2004), Relocation of the eastern Taiwan earthquakes and its tectonic implications, *Terr. Atmos. Oceanic Sci.*, *15*, 647–666.

Kuochen, H., Y. M. Wu, Y. G. Chen, and R. Y. Chen (2006), 2003 *Mw*6. 8 Chengkung earthquake and its related seismogenic structures, *J. Asian Earth Sci.*, in press.

Lee, J. C., J. Angelier, H. T. Chu, J. C. Hu, and F. S. Jeng (2001), Continuous monitoring of an active fault ina plate-suture zone: A creepmeter study of the Chihshang active fault, eastern Taiwan, *Tectonophysics*, *333*, 219–240.

Lee, J. C., J. Angelier, H. T. Chu, J. C. Hu, F. S. Jeng, and R. J. Rau (2003), Active fault creep variations at Shihshang, Taiwan, revealed by creep meter monitoring, 1998–2001, *J. Geophys. Res.*, *108*(B11), 2528, doi:10.1029/2003JB002394.

Okada, Y. (1992), Internal deformation due to shear and tensile faults in a half-space, *Bull. Seismol. Soc. Am.*, *82*, 1018–1040.

Shyu, J. B. H., K. Sieh, and Y. G. Chen (2005), Tandem suturing and parting of the Taiwan orogen revealed by its neotectonic elements, *Earth Planet. Sci. Lett.*, *233*, 167–177.

Suppe, J. (1981), Mechanics of mountain buiding in Taiwan, *Mem. Geol. Soc. China*, *4*, 67–89.

Teng, L. S. (1990), Geotectonic evolution of late Cenozoic arc-continent collision in Taiwan, *Tectonophysics*, *183*, 57–76.

Tsai, Y. B. (1986), Seismotectonics of Taiwan, *Tectonophysics*, *125*, 17–38.

Yu, S. B., and L. C. Kuo (2001), Present-day crustal motion along the Longitudinal Valley Fault, eastern Taiwan, *Tectonophysics*, *333*, 199–217.

Yu, S. B., and C. C. Liu (1989), Fault creep on the central segment of the Longitudinal Fault, eastern Taiwan, *Proc. Geol. Soc. China*, *32*, 209–231.

Yu, S. B., D. D. Jackson, G. K. Yu, and C. C. Liu (1990), Dislocation model for crustal deformation in the Longitudinal Valley area, eastern Taiwan, *Tectonophysics*, *183*, 97–109.

Yu, S. B., H. Y. Chen, and L. C. Kuo (1997), Velocity field of GPS stations in the Taiwan area, *Tectonophysics*, *274*, 41–59.



C. H. Chang, H. Kuochen, T. C. Shin, and C. F. Wu, Central Weather Bureau, Taipei 100, Taiwan.

Y. G. Chen, J. C. Hu, and Y. M. Wu, Department of Geosciences, National Taiwan University, Taipei 106, Taiwan. (ygchen@ntu.edu.tw)

C. S. Hou, Central Geological Survey, Taipei 235, Taiwan.

T. L. Teng, Department of Earth Sciences, University of Southern California, Los Angeles, CA 90089, USA.